Sacchet *et al. Energy Mater.* **2025**, *5*, 500042
DOI: 10.20517/energymater.2024.112

Energy Materials

Article

Open Access

Check for updates

High density polyethylene with phase change materials for thermal energy management

Sereno Sacchet[1,*], Francesco Valentini[1], Caterina Rizzo[2], Riccardo Po[3], Luca Fambri[1,*]

[1]Department of Industrial Engineering, University of Trento and INSTM Research Unit, Trento 38123, Italy.
[2]Renewable, New Energies and Material Science Research Center, San Donato Milanese I-20097, Italy.
[3]Renewable, New Energies and Materials Science Research Center, "Istituto Guido Donegani", Novara 28100, Italy.

***Correspondence to:** Dr. Sereno Sacchet, Department of Industrial Engineering, University of Trento and INSTM Research Unit, via Sommarive 9, Trento 38123, Italy. E-mail: sereno.sacchet@unitn.it; Prof. Luca Fambri, Department of Industrial Engineering, University of Trento and INSTM Research Unit, via Sommarive 9, Trento 38123, Italy. E-mail: luca.fambri@unitn.it

How to cite this article: Sacchet, S.; Valentini, F.; Rizzo, C.; Po, R.; Fambri, L. High density polyethylene with phase change materials for thermal energy management. *Energy Mater.* **2025**, *5*, 500042. https://dx.doi.org/10.20517/energymater.2024.112

Received: 6 Aug 2024 **First Decision:** 6 Nov 2024 **Revised:** 21 Nov 2024 **Accepted:** 4 Dec 2024 **Published:** 26 Jan 2025

Academic Editor: Yuping Wu **Copy Editor:** Fangling Lan **Production Editor:** Fangling Lan

Abstract

Phase change materials (PCMs) represent an innovative solution to passively manage device temperature or store heat, taking advantage of the material phase transitions. In this work, the attitude of high density polyethylene (HDPE) for the shape stabilization of three selected organic PCMs with a melting temperature close to 55 °C was investigated. Composites with PCM content in the range of 50-61 wt.% were produced by melt compounding, and lab-scale panels were produced by compression molding. The ability of the supporting olefinic matrix to stabilize the PCM and contain leakage was verified and compared through thermo-mechanical characterization. Moreover, expanded graphite was introduced according to a novel vacuum impregnation process in order to provide an extra stabilizing contribution, resulting in an outstanding thermal conductivity increase of up to 1.6 W/m·K, and a maximized enthalpy of 112 J/g. Besides the shape stability, HDPE also improves the mechanical properties of PCM-based composites, as documented by detailed and extended characterization through cold and hot compression tests, flexural tests, Vicat and shore A tests. The thermal management effect of the materials is quantified through infrared thermography, by proportionally relating the temperature lags to the high melting/crystallization enthalpy of the investigated products. In view of thermal management applications in the range of 30-60 °C, the main properties of selected HDPE panels with different PCMs are summarized and compared.

Keywords: High density polyethylene, phase change materials, thermal management, thermal energy storage, expanded graphite, thermal conductivity, mechanical properties

INTRODUCTION

Phase Change Materials (PCMs) are latent heat storage materials able to absorb an incoming heat flux and store thermal energy at a constant temperature once the melting point is reached. The heat stored by the material is released during crystallization, always maintaining a constant temperature until the phase transition is completed[1]. PCMs are employed in several applications related to the energetic transition, necessary for the reduction of global warming and greenhouse gas emissions. They can be used to smooth temperature peaks in batteries for overheating prevention[2,3], to enhance the energy efficiency of building environments[4,5] or to be combined with photovoltaic (PV) generation in active or passive latent heat systems, respectively, to store the heat surplus or contain the efficiency loss of silicon PV panels with the temperature rise[6,7].

PCMs are subdivided into classes depending on the chemical structure. The most widely employed are the organic materials, typically paraffins, fatty acids and poly(ethylene glycol) derivatives. They present chemical stability and reliability, non-corrosiveness and relatively high melting enthalpy, in the range of 150-270 J/g[8]. However, they are also flammable, exhibit a consistent volume expansion upon melting and present low thermal conductivity. The most representative inorganic PCMs are metals and alloys, salts and salts hydrated. They are cheap, not flammable and have high thermal conductivity. However, salt-based PCMs are characterized by poor stability, corrosiveness and possible supercooling phenomena. In order to precisely tune the operating temperature of PCMs, eutectic mixtures (organic-organic, inorganic-inorganic or organic-inorganic) can be exploited[9].

The main issue regarding organic PCMs is their confinement once molten, which can be solved using macro- or micro-encapsulation[10] or realizing a shape stabilization by dispersing them into polymeric supporting matrixes, such as thermoplastic elastomers[11], acrylic resins[12] or ethylene propylene diene monomer (EPDM) rubber[13].

Among thermoplastic polymers, high density polyethylene (HDPE) emerges as one of the best candidates for its chemical and structural similarities with paraffinic PCMs, guaranteeing not only compatibility and miscibility[14], but also a suitable processability temperature, lower than degradation onset temperature of PCMs. The low thermal conductivity of organic PCMs must be increased to ensure proper heat transfer in both thermal management and Thermal Energy Storage (TES) applications, conferring faster charging/discharging rates; the addition of carbon nano-structured materials as graphene[15], graphene oxide[16] or expanded graphite (EG)[17] is one of the most effective strategies to improve performances for thermal energy storage[18], also in combination with a polymeric supporting matrix[19-21]. The porous structure of carbon-based materials facilitates effective stabilization of PCMs thanks to their interlamellar intercalation, especially using EG, which is advantageous due to its low density, high specific surface area and lower cost than the other carbonaceous fillers[15,18,22-24]. Moreover, even a small fraction of EG can significantly enhance thermal conductivity, while effectively containing leakage of the high enthalpy PCM-based composite material[23].

In the open literature, despite the existence of several works investigating PCM stabilization using HDPE[20-22,25-27], mechanical properties have not been properly documented and the enhancement conferred by the thermoplastic matrix has not been considered. In some cases, small amounts of HDPE are introduced as a nucleating agent to contain the supercooling phenomenon in active latent heat storage, where shape stabilization is not required[24,28-31], such as in TES applications[32]. Moreover, HDPE has also been recently suggested in combination with bio-based fillers such as wood flour[33], beech[34] or nanocellulose[35] to create eco-friendly solutions. However, this comes at the expense of significantly lowering the enthalpy of

transition in the range of 18-76 J/g, especially in the case of PCM microcapsules[36,37].

This research contribution is part of a larger study by the authors dedicated to the development of materials for the thermal management of silicon PV cells, extending the variety of PCMs having melting temperatures close to 55 °C, as documented in our previous work[23]. Photovoltaics (PV) is one of the most developed renewable technologies in energy conversion, and today, 97% of the PV market consists of mono- and poly-crystalline silicon cells[38,39]. In addition, cumulative PV installations are continuously growing, making it increasingly difficult for emerging PV technologies to fully replace silicon ones, which offer advantages such as low cost, economies of scale and environmental benefits[40]. Silicon cell efficiency is approaching the maximum theoretical value, making it extraordinarily relevant to avoid the efficiency losses caused by temperature rise, especially in regions where irradiances are very intensive and temperatures can easily exceed 40 °C[41].

In particular, this study examines the interaction of HDPE with three PCMs of different natures, investigating the use of a HDPE matrix in the PCM shape stabilization. A double stabilization approach using HDPE and EG is also explored to enhance thermal conductivity and maximize melting enthalpy, avoiding any loss of PCMs. Furthermore, the mechanical properties of the materials and the produced panels have been adequately considered, filling the lack of detailed studies in the literature. The final applications can be considered versatile and no longer exclusively related to the thermal management of PV cells, leaving room for other electronic devices or TES applications with the advantage of proper shape retention above PCM melting and improved mechanical properties.

EXPERIMENTAL

Materials

Three organic PCMs with melting points near 55 °C were investigated. The first one was an organic aliphatic compound, Rubitherm® RT54HC (RT), with a melting point of 54 °C, a melting enthalpy of 200 J/g, and a density of 0.80 g/cm^3 at the liquid state, provided by Rubitherm GmbH (Berlin, Germany). The second was a bioderived and biodegradable PCM, Puretemp® PT58X (PT), with a melting point of 58 °C, a melting enthalpy of 225 J/g, a thermal conductivity of 0.2 W/m·K and a density of 0.81 g/cm^3 at the liquid state, provided by PureTemp (Minneapolis, United States). The third was a bioderived mixture of fatty acids, specifically stearic and palmitic acids, commercially known as FATTY ACIDS C16-18 (SP), with a melting point of 55 °C, a melting enthalpy of 200 J/g and a density of 0.89 g/cm^3 at the liquid state, provided by Carlo Erba Reagents (Val De Ruil, France). HDPE was used as a matrix for the PCM shape stabilization. The product PLASTENE® AD25 in the form of fine powder, with a density of 0.955 g/cm^3 at 23 °C and a melt flow index (MFI) of 25 g/10 min (at 190 °C, 2.16 kg), was provided by Poliplast S.p.A. (Casnigo, Italy). A commercial expanded graphite SIGRAFLEX® EXPANDAT by SGL CARBON GmbH (Meitingen, Germany) with a tapped density of 25 g/L at 20 °C and a particle size of 4-40 μm was selected as a filler to improve the thermal conductivity.

Samples preparation

The first production step involved impregnating EG with PCM using a rotary evaporation apparatus, as extensively described in a previous work[23]. PCM was manually stirred adding 12.7 wt.% of EG, which corresponds to 14 phr (parts per hundred ratio), optimum amount for both shape stabilization and thermal conductivity enhancement[23]. 114 g of the dispersed mixture were inserted in a 1 L flask, which was connected to the rotary evaporator.A vacuum of 60 mbar was applied while continuing the mixing at a fixed rotation speed of 20 rpm at room temperature. After 5 min, the flask was placed in a water bath, heated to 90 °C, and the rotation was maintained for 30 min after the PCM melting to allow the complete absorption

Table 1. Samples coding and compositions for preliminary tests

Sample code	RT (wt.%)	PT (wt.%)	SP (wt.%)	HDPE (wt.%)	EG (wt.%)
RT/EG14	87.7	-	-	-	12.3
PT/EG14	-	87.7	-	-	12.3
SP/EG14	-	-	87.7	-	12.3

Table 2. Samples underwent full characterization. Code and relative nominal compositions in wt.% of the produced HDPE composites after melt compounding of PCM with HDPE and compression molding. SP/EG14 was initially produced by rotavapor impregnation

Sample code	RT (wt.%)	PT (wt.%)	SP (wt.%)	HDPE (wt.%)	EG (wt.%)
PE-50RT	50	-	-	50	-
PE-50PT	-	50	-	50	-
PE-50SP	-	-	50	50	-
PE-70SP/EG14*	61.4	-	-	30	8.6

*Two PCM-EG compositions were prepared with and without rotavapor stabilization. Only the composition with rotavapor stabilization underwent full characterization.

of the PCM within the EG matrix. After cooling outside the bath, the vacuum and rotation were removed, resulting in powdery stabilization of PCM within the EG. Preliminary tests for selecting the PCM to which the conductive filler would be added were performed on vacuum-impregnated PCM/EG samples, as listed in Table 1.

HDPE-stabilized PCM composites were prepared through melt compounding followed by hot compression molding: (i) using the PCMs without stabilization; and (ii) using one of the stabilized PCMs (SP).

The precursors were weighted with balance Kern KB3600 (sensitivity 0.01 g) and compounded using a Thermo Haake Rheomix 600 (Thermo Fisher Scientific, USA) equipped with counter-rotating rotors. The compounding process was performed at 135 °C for 8 min with only HDPE, followed by an additional 5 min after the addition of the PCMs. The rotor speed was 50 rpm and the total amount of material inserted into the mixer chamber was 50 g. The obtained blends were then pressed using a Carver hot press at 140 °C, with a pressure of 2.5 MPa for 5 min. The material was put between two stainless steel plates inside a mold having a frame of different dimensions: 40 × 40 × 10 mm^3, 12 × 12 × 3 mm^3 and 200 × 200 × 3 mm^3. Water cooling to room temperature for 5 min was conducted before the remotion of the obtained sheets from the press.

Samples containing 50 wt.% of HDPE and complementary weight fraction of the three PCMs without EG stabilization were produced. In the case of EG-stabilized PCM (SP only), a composition with 30 wt.% of HDPE was prepared. In order to verify the effective necessity of SP vacuum impregnation, which permits the PCM intercalation between the graphitic lamellae, direct insertion of EG in the compounder (without rotavapor stabilization) was also performed, producing the sample PE-70SP/EG14 (no rot), which showed abundant PCM loss, as confirmed by differential scanning calorimetry (DSC). The four compositions selected for the full characterization are listed in Table 2.

A 90 μm thick polyethylene (PE) envelope for alimentary applications, provided by ORVET S.p.A. (Musile di Piave, Italy), was thermo-welded using an under-vacuum thermo-welding machine ORVET VM-16 in order to totally avoid PCM leakage.

Experimental methodologies

Preliminary tests

The selected PCMs were compared by Fourier-transform infrared spectroscopy (FTIR) in order to investigate the chemical structure. Spectra were obtained by using the spectrometer Spectrum One (Perkin-Elmer) operating in Attenuated Total Reflection (ATR) mode in a wavenumber range from 4,000 to 640 cm^{-1} by averaging four scans.

The interaction of EG with the three PCMs and its ability to stabilize them was investigated through leakage tests on disks with a mass of 1 g, a diameter of 20 mm and a density of 1 g/cm^3. These disks were obtained through cold compaction of the 14 phr EG rotavapor-impregnated powder, applying 10 MPa for 30 s. The disks were placed on filter paper into an oven at 60 °C for 3 h, with mass loss monitored hourly. In this manner, the best PCM stabilized through EG impregnation could be determined.

Full characterization

Thermogravimetric analysis (TGA) from 30 to 700 °C at a 10 °C/min heating rate under a 10 mL/min air flow was conducted using a Mettler TG50 thermobalance (Mettler-Toledo, Switzerland) equipped with an alumina crucible. The temperatures associated with a mass loss of 5 wt.% ($T_{5\%}$), the temperature of maximum degradation rate (T_{peak}) as the peak of derivative thermogravimetric analysis (DTGA), and the residual mass at 350 °C (m_{350}), 400 °C (m_{400}) and 700 °C (m_{700}) were determined.

DSC of neat PCMs and HDPE-based composites was performed using a Mettler DSC30 calorimeter, under a nitrogen flow (100 cm^3/min) with a thermal cycle of heating/cooling/heating in the range of 30 to 60 °C into 40 μL aluminum crucibles. This scanning rate of 1 °C/min was selected to precisely determine the phase transition ranges[23,42]. The melting temperatures during the first and the second heating scans (T_{m1} and T_{m2}), the crystallization temperature (T_c) and the specific melting and crystallization enthalpy values (ΔH_{m1}, ΔH_c and ΔH_{m2}) were obtained. The effective PCM content in the second heating scan (PCM_{m2}^{eff}) was determined as the ratio of the specific enthalpy of the specimens and the corresponding specific enthalpy of the neat PCM, as given in

$$PCM_{m2}^{eff} = \frac{\Delta H_{m2}}{\Delta H_{m2,PCM}} \cdot 100 \quad (1)$$

while the efficiency of melting during the second heating scan (η_{m2}) was evaluated using

$$\eta_{m2} = \frac{\Delta H_{m2}}{\Delta H_{m2,PCM} \cdot W_{PCM}} \cdot 100 \quad (2)$$

where $\Delta H_{m2,PCM}$ is the specific enthalpy value associated with melting during the second heating scan of neat PCM, while W_{PCM} is the PCM weight fraction. The parameters expressed in Equations (1) and (2) represent the main indicators to verify the suitability for the PCM stabilization, affected by composition and production processes.

The ability of the produced composite sheets to retain PCM was investigated through leakage tests. These tests involved monitoring the weight of 120 × 120 × 3 mm^3 sheets placed into an oven at 60 °C on an absorbent paper towel for 40 days. The residual PCM content was calculated as weight percentage with respect to the total specimen weight, considering the initial PCM percentage at the beginning of the test, i.e., the effective PCM content, as determined according to Equation (2) by the melting enthalpies in DSC tests;

the entire weight loss over time was associated with the PCM leakage.

Scanning electron microscopy (SEM) observations of cryo-fractured samples were performed to observe the phase distribution, using a Zeiss Supra 40 field emission scanning electron microscope operating in vacuum at 10^{-6} Torr, equipped with a secondary electron detector and working at an acceleration voltage of 2.5 kV. Before the observations, the fracture surfaces of the specimens were metalized through the deposition of a thin electrically conductive coating of Pt-Pd inside a vacuum chamber.

The apparent density (ρ_{exp}) of the samples was measured using an Ultrapyc 5000 helium pycnometer (Anton Paar, Austria) at 23 °C. For each sample 30 measurements were performed using a testing chamber of 4.5 cm^3. The theoretical density (ρ_{th}) was evaluated by considering the weight percentage of the phases from DSC and using the measured densities of the PCMs and HDPE for the respective phases. For graphite, the theoretical density of 2.26 g/cm^3 was used[23].

The void fraction (ϑ_v) was computed using

$$\vartheta_v = \frac{\rho_{th} - \rho_{exp}}{\rho_{th}} \cdot 100 \tag{3}$$

The specific heat capacity at constant pressure (c_p) was determined at 30 °C following the ASTM E1269-11 standard[43]. This method involves comparing DSC curves obtained from the sample with those from a sapphire reference of known specific heat capacity. Three specimens for each sample were analyzed using a Mettler DSC30 machine, performing 4 min of isotherm at 20 °C, followed by heating at 5 °C/min till 40 °C and other 4 min of isotherm at the final temperature.

Thermal diffusivity (α) of neat PCMs and blends at 30 °C was determined with two different techniques, using:

• a Neztsch Laser Flash Analyzer (LFA) 446 on disks with a 12.7 mm diameter and a 2.5 mm thickness, imposing laser signals of 250 V for a pulse width of 0.6 ms;

• a Hot Disk thermal analyzer, equipped with a 7577 sensor (diameter of 4.002 mm) on approximatively 40 × 40 × 10 mm^3 specimens, according to ISO 22007 standard[44] into a Memmert HCP climatic chamber at fixed 30% relative humidity applying for 1 to 3 s a power of 30 to 50 mW.

Three specimens for each sample were analyzed. Thermal conductivity (λ) at 30 °C was indirectly determined as product of thermal diffusivity α, bulk density of specimens ρ (measured as ratio between mass and geometrical volume) and the specific heat capacity c_p, as given in

$$\lambda = \alpha \cdot \rho \cdot c_p \tag{4}$$

Thermal conductivity values were distinguished as λ_{HD} and λ_{LFA}, depending on whether they were determined using the hot disk technique or LFA, respectively. The uncertainties were calculated considering the error propagation.

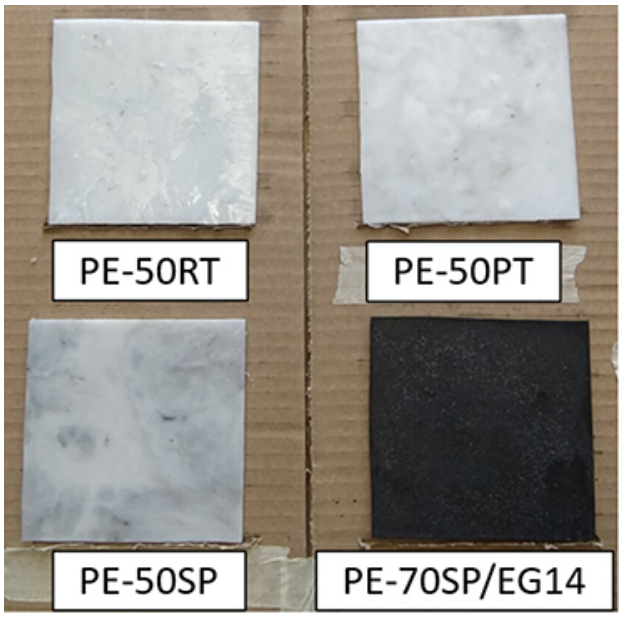

Figure 1. Sheets of PCM-HDPE composites (120 × 120 × 3 mm^3) placed on a paperboard and observed with IR thermography.

The mechanical behavior of the PE macro-encapsulated materials was evaluated through compression tests of 40 × 40 × 10 mm^3 specimens using an Instron 5969 testing machine equipped with a load cell of 10 kN and a thermostatic chamber to perform the tests at 30 and 80 °C, above and below the melting temperature of the PCM, respectively. The tests were performed on neat HDPE and samples containing PCM at a rate of 1 mm/min, following the standard ISO 844[45] (with different specimen geometries adapted to the specific case). From the obtained stress-strain curves, the compressive modulus of elasticity (E_C) in the linear part of the curve between 4% and 7% of strain and the stress at 10% of deformation (σ_{10}) were evaluated. The strain at 5 MPa (ε_5) was computed for the tests conducted at 30 °C, while for the tests at 80 °C, the strain at 0.5 MPa ($\varepsilon_{0.5}$) was selected due to the different responses of the specimens below or above the PCM melting point. Furthermore, the stress at 20% of deformation (σ_{20}) was evaluated at 80 °C. The results represent the average of three specimens.

Three-point bending tests were performed at 23 °C using an Instron 5969 dynamometer equipped with 1 kN load cell, following the ASTM D790-17 standard[46], by using bars of 80 × 10 × 4 mm^3 and the testing rate of 1.7 mm/min. From the obtained stress-strain curves, the flexural elastic modulus (E_f) was determined in the strain range of 0.1%-0.4%, while the flexural strength (S_f) and flexural strain at break (ε_{fb}) were determined at the maximum load as the average of three specimens.

Vicat softening temperature (*VST*) was determined following ASTM D1525-17e1 standard[47] using a HDT-Vicat tester model MP/3 subjecting small bars of 4 mm thickness to a mass of 10 N and heating rate of 2 °C/min. The results represent the average of three specimens.

Shore A hardness was determined at 30 and 80 °C using a Hildebrand durometer with an applied load of 488 g for a duration of 5 s, performing ten measurements for each sample, following ASTM D2240[48].

Finally, infrared (IR) thermography was conducted to observe the PCM homogeneity in the samples and observe the heating and cooling delay of sheets 120 × 120 × 3 mm^3 subjected to a thermal cycle from 23 °C

(room temperature) to 84 °C imposed into an oven, using an IR thermal imaging camera IRtech Fotric 348A. The sheet configurations to be compared in thermography are shown in Figure 1. During heating, the frames were acquired after at least 20 s from the paperboard removal from the oven.

RESULTS AND DISCUSSION

Preliminary comparison of PCMs and leaking tests on EG-stabilized PCMs

The three selected PCMs were compared by FTIR analysis, as shown in Figure 2. RT, a modified organic aliphatic compound (RT54HC), was identified by the aliphatic C-H stretching peaks at about 2,915 and 2,850 cm^{-1}, and bending and wagging peaks at about 1,470 and 725 cm^{-1}. Additionally, the intense peak at about 1,700 cm^{-1}, attributed to C=O stretching, and the broad band between 2,600 and 2,550 cm^{-1} typical of -COOH, together with its close similarity to SP in the fingerprint zone (discussed later), suggest an attribution to aliphatic fatty acids.

The spectrum of PT is consistent with that of aliphatic alcohol, showing the -OH stretching in the range 3,400-3,050 cm^{-1}, the C-O stretching at 1,060 cm^{-1}, and the other three main double peaks of -CH_2-CH_2-, i.e., stretching at 2,920-2,850 cm^{-1}, bending at 1,470-1,455 cm^{-1} and wagging at 720 cm^{-1}.

Fatty acid mixture SP is derived from stearic and palmitic acids. As expected, the FTIR spectrum exhibits the C=O stretching peak at about 1,700 cm^{-1}, and the typical band at 2,700-2,500 cm^{-1} of -COOH, plus the signals of various -CH_2- and -CH_3. The near-equivalence of the SP and RT spectra suggests a qualitatively identical composition, with probably some minor quantitative differences. The EG ability to stabilize the different PCMs is investigated considering the three-hour long leakage test results on pressed disks of vacuum-impregnated EG with PCMs [Figure 3].

A better interaction between SP and RT (both aliphatic fatty acids) and EG is evident compared to the behavior of PT, an aliphatic fatty alcohol. In the first hour, PT/EG14 shows a mass loss more than three times greater than that of the other two samples. Over the following 2 h, the trend becomes similar for all disks. After 3 h of testing, the total mass loss of RT/EG14 and SP/EG14 is 2.4 and 1.8 wt.%, respectively, indicating SP/EG14 is the best candidate for EG introduction into the HDPE-based composites; in addition, SP can be considered more sustainable as it is bio-derived. The better EG stabilization of the fatty acid mixture (SP and RT) compared to the aliphatic alcohol (PT) is likely due to the higher chain polarity and capillarity forces conferred by the carboxylic group, resulting in a quite stable PCM/EG interaction[23].

Thermogravimetric analysis

Thermogravimetric analysis (TGA) curves of neat PCMs, neat HDPE and composite samples as residual mass and derivative of thermogravimetric analysis (DTGA) are reported [Figure 4]. Main results are summarized in Table 3: temperatures associated with a mass loss of 5 wt.% ($T_{5\%}$), temperatures associated with the maximum rate of degradation (T_{peak}) with multiple peaks for HDPE composites, and the residual masses at 700 °C (m_{700}). The full thermal degradation of PCM is clearly evident in the range 200-300 °C, with a faster mass loss for aliphatic alcohol (PT) compared to aliphatic acids. The maximum degradation rates (DTGA peaks) center at 226 and 287 °C, respectively. On the other hand, the main degradation of HDPE occurs above 400 °C, and the produced composites show intermediate behavior, with a two-step degradation evidenced by two peaks in DTGA, attributable to PCM and the polymeric matrix, respectively.

The PCMs begin degradation at around 200 °C, with PT showing lower resistance to temperature ($T_{5\%}$ 204 °C), whereas RT and SP exhibit similar and higher values ($T_{5\%}$ 227 °C). This confirms PCM stability during processing at 140 °C. Above 400 °C, all the PCMs completely degrade with no residual masses at the end of

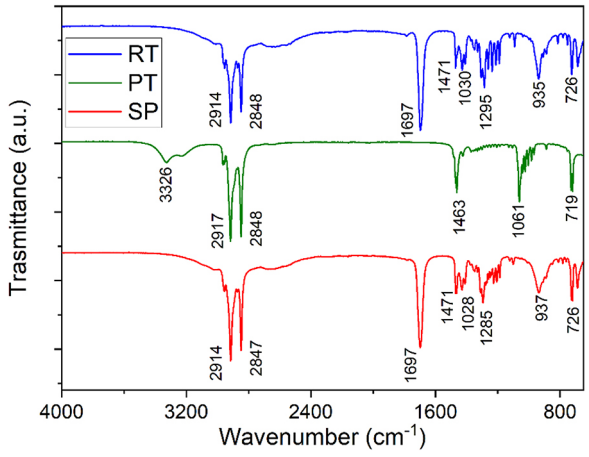

Figure 2. FTIR spectra of RT, PT and SP phase change materials with melting temperature of about 55 °C.

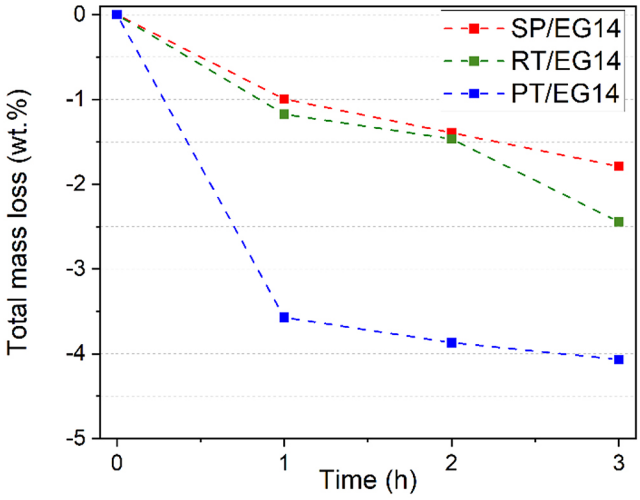

Figure 3. Leakage test results at 60 °C of vacuum-impregnated EG with PCMs.

Table 3. TGA results of neat PCMs, composite samples and neat HDPE

Sample	$T_{5\%}$ (°C)	T_{peak} (°C)	m_{350} (%)	m_{400} (%)	m_{700} (%)
RT	226.8	287.5	0.5	0.3	0.0
PT	203.8	265.5	2.2	1.5	0.0
SP	226.7	289.2	3.4	2.6	0.0
PE-50RT	211.5	257.7 – 444.2	52.8	44.9	0.0
PE-50PT	226.3	253.7 – 425.5	58.3	54.4	0.0
PE-50SP	246.3	300.7 – 444.5	57.2	44.9	0.0
PE-70SP/EG14	232.0	296.5 – 489.2	34.0	26.6	8.1
HDPE	357.3	433.8	95.1	91.8	0.0

$T_{5\%}$: Temperatures associated with a mass loss of 5 wt.%; T_{peak}: temperatures associated with the maximum degradation rate as the peak of DTGA; m_{350}: residual mass at 350 °C; m_{400}: residual mass at 400 °C; m_{700}: residual mass at 700 °C.

the tests. HDPE starts thermal degradation above 300 °C, with 5 wt.% of degradation at 357 °C and a peak of weight loss at 434 °C, with the complete mass loss at about 550 °C. Two degradation peaks appear for the

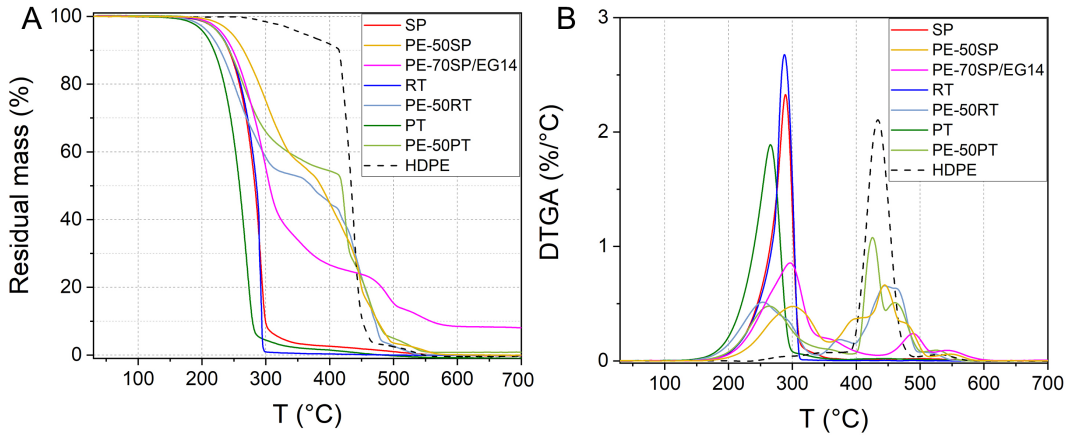

Figure 4. TGA of neat PCMs, composite samples and neat HDPE. (A) Residual mass; (B) Derivative thermogravimetric analysis (DTGA).

samples PE-50RT, PE-50SP and PE-50PT. The first peak corresponds to the degradation of the PCM (T_{peak} respectively at 258, 301 and 254 °C), followed by the degradation of HDPE (442, 443 and 426 °C). The mass loss at 350-400 °C could be considered a semiquantitative evaluation of PCM content, i.e., about 45%-50% in PE-50PCM, and about 60% in PE-70SP/EG14, partially agreeing with the nominal content.

No residues for PCMs, HDPE and their compositions at 50 wt.% are found at 700 °C due to the complete thermal degradation. On the other hand, PE-70SP/EG14 shows a residual mass of 8.1 wt.%, almost corresponding to the nominal content of EG, which is stable at 700 °C[23]. This double-stabilized sample presents a more gradual mass loss profile, due to the presence of three distinct phases degrading at three different temperatures.

Differential scanning calorimetry

Phase transition temperatures and enthalpies of neat PCMs can be determined from the Differential Scanning Calorimetry (DSC) thermograms as shown in Figure 5, and the main results are summarized in Table 4.

As shown in Figure 5, the entire melting transition occurs in the range 49-58 °C, while the crystallization peaks during cooling are observed in the range of 54-43 °C. According to the declared melting temperatures from the datasheets, there is a shift of a few degrees to higher temperatures as the transition occurs from fatty acids (RT and SP) to fatty alcohol (PT). PT shows the highest enthalpic content (250 J/g), making it preliminarily the best among the three PCMs, with its melting enthalpy much higher than that of RT (206 J/g) and SP (196 J/g). PT, whose composition is not specified by the producer, presents a double crystallization peak at 53 and 47 °C, respectively, indicating the probable presence of two distinct phases of fatty alcohol. It also shows among the three PCMs, the broadest temperature interval for crystallization, ranging from 54 to 43 °C.

Figure 6 displays the DSC thermograms of the HDPE composite samples, including melting, crystallization and melting during the second scan. Selected data of enthalpy and temperature transitions are provided in Table 5.

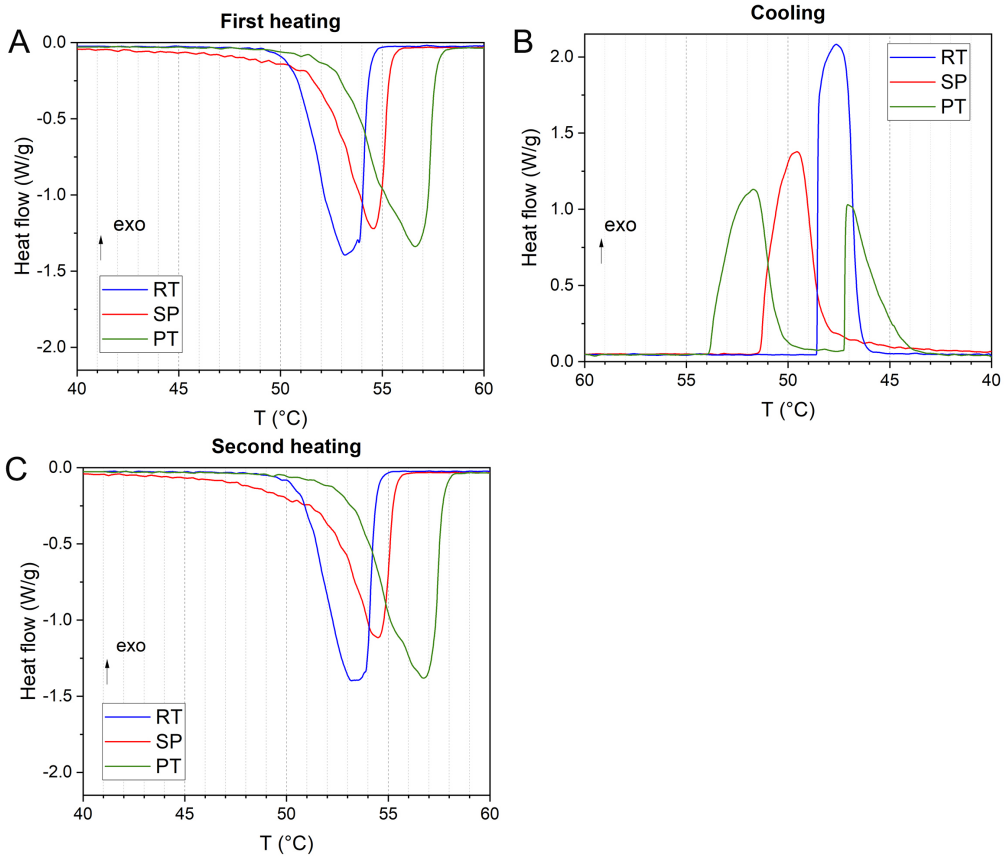

Figure 5. DSC thermograms of the neat PCMs at 1 °C/min. (A) First heating; (B) Cooling; (C) Second heating. Fatty acids (RT and SP) and fatty alcohol (PT).

Table 4. Selected DSC data of the investigated PCMs: two fatty acids (RT and SP) and one fatty alcohol (PT)

Sample	T_{m1} [°C]	ΔH_{m1} [J/g]	T_c [°C]	ΔH_c [J/g]	T_{m2} [°C]	ΔH_{m2} [J/g]
RT	51.5	204.0	50.1	205.9	51.6	206.3
PT	54.9	250.6	53.1 / 47.4	249.3	55.0	249.9
SP	53.4	196.5	50.9	193.2	53.4	195.8

Melting temperature and enthalpy in the first (T_{m1} , ΔH_{m1}) and second heating (T_{m2} , ΔH_{m2}), crystallization temperature and enthalpy (T_c , ΔH_c).

Table 5. Selected DSC results of HDPE-stabilized PCM samples. Temperature and transition values in heating and cooling; effective PCM content and efficiency of melting according to Equations (1) and (2)

Sample	T_{m1} [°C]	ΔH_{m1} [J/g]	T_c * [°C]	ΔH_c [J/g]	T_{m2} [°C]	ΔH_{m2} [J/g]	PCM_{m2}^{eff} [%]	η_{m2} [%]
PE-50RT	51.9	94.0	49.7/43.0/38.0	88.1	51.3	91.6	44.4	88.8
PE-50PT	55.3	96.7	53.0/47.6/32.9	89.5	54.6	95.1	38.1	76.1
PE-50SP	53.0	55.1	51.0/45.4	48.5	52.9	49.3	25.2	50.4
PE-70SP/EG14	54.0	116.2	51.5/46.1	112.4	54.0	112.1	57.3	93.2
PE-70SP/EG14 (no rotavapor)	53.0	87.3	51.3/46.8	85.5	53.1	86.0	43.9	71.5

*Shoulder peaks and different temperatures are reported (see comments in the text).

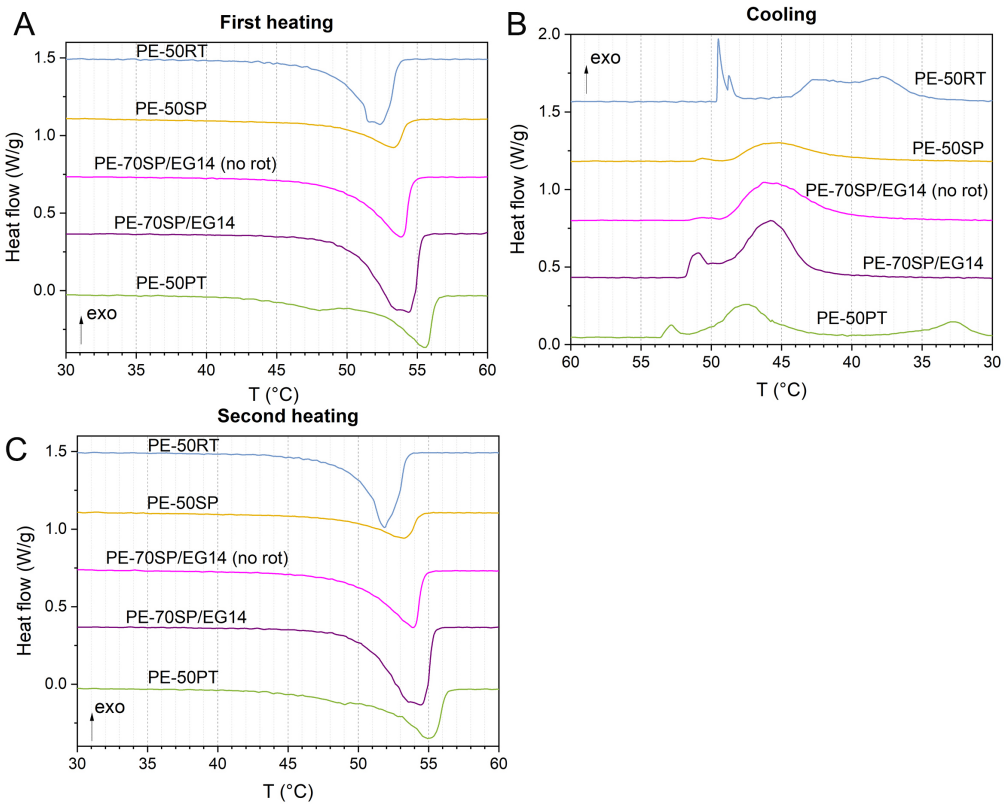

Figure 6. DSC thermograms of the HDPE-based samples at 1 °C/min. (A) First heating; (B) Cooling; (C) Second heating.

The melting temperature of the main peaks is in the range 52-54 °C, quite similar to the corresponding neat PCMs. However, it is worth noting that a relatively larger interval of PCM melting in HDPE compositions with the presence of shoulder peak, in both heating scans [Figure 6A and C], suggests the formation of different crystal domains.

Concerning crystallization, a broadening of the phase transition is observed [Figure 6C], with multiple peaks for the various PCMs in HDPE. It is also evident that the main peaks exhibit a lower crystallization temperature compared to those of pure PCMs. For instance, the main peak of crystallization of SP in HDPE is at 45 °C, instead of 51 °C [Table 4], showing a shoulder at about 50 °C. Moreover, three peaks were observed for PE-50RT (50, 43 and 38 °C) and PE-50PT (53, 48 and 33 °C) indicating HDPE inhibits crystallization, as demonstrated in other studies[49,50]. Similar multiple melting peaks were documented for co-crystallization of syndiotactic polystyrene (sPS) in PA66[51] and were attributed to the dispersed particles. The lower the size domain in the surrounding polymeric matrix, the lower the perfection of crystals and the lower the melting temperature. These findings were interpreted by Michell and Muller as fractionated crystallization upon cooling from the melt due to confinement effect, reduction in lamellar thickness, and decrease in melting temperature[52]. Noteworthy in this context is the main crystallization peak of SP after impregnation in EG and dispersion in HDPE, which shifts from 53 to 46 °C, with a minor peak remaining at about 51 °C [Figure 6B and Table 5].

The energy involved in the thermal process was evaluated in the second heating scan by the melting enthalpy and the efficiency of melting [Table 5 and Equation (2)]. The first three compounds with a nominal content of PCM at 50 wt.% resulted in effective PCM content in the range 25-44 wt.% according to

Equation (1). In particular, the lowest melting enthalpy (49 J/g for PE-50SP), with an efficiency η_{m2} of 50%, is unacceptable in terms of material application. These results could be attributed to PCM loss during production, especially during pressing, and the reduced dimensions and imperfections of crystalline domains. A similar enthalpy reduction was observed in PCM dispersed in wood-based composites as a result of spatial confinement effects on PCM[53].

Although enthalpies are significantly reduced compared to neat PCMs due to the presence of the matrix, values of 92 and 95 J/g can be obtained for PE-50RT and PE-50PT, corresponding to melting efficiencies of 89% and 76%, respectively. This evidence a better ability of RT than PT to be stabilized in HDPE through the considered production process.

A significant improvement in the efficiency of SP in HDPE compounds was achieved through EG impregnation. In fact, graphite can provide a strong stabilizing effect due to capillary forces and surface tensions[23], notwithstanding its low fraction (8.6 wt.%) in the composite. Effective PCM content increased up to 44% (86 J/g) after the direct insertion of the graphitic filler into the compounder, and to 57% (112 J/g) after rotavapor process, which is very close to the nominal value of 61%. For these reasons, PE-70SP/EG14, produced after vacuum impregnation of the EG, exhibited the highest efficiency (93%) and was selected for the subsequent characterizations. These enthalpy values are very promising and higher than those reported in many works exploring PCM shape stabilization using HDPE (10-66 J/g), as in the case of wood fiber composites 60 J/g[54], or in combination with EG[14,36,55] or other graphitic fillers[20]. The DSC analysis results quantify the ability of PCM systems to subtract heat from a device in thermal management applications and store heat in TES.

Leakage test

The ability of HDPE composites to retain the PCM above its melting temperature over time was assessed through a leakage test performed at 60 °C for 40 days, as shown in Figure 7, which illustrates the PCM content in wt.% of the four samples as a function of time. The initial value corresponds to the effective PCM content from Table 5, and the final PCM loss is reported in the caption. A comparison of the leakage of PE-70SP/EG14 and PE-50PT sheets at the end of the test is shown in the pictures.

The PCM loss is concentrated in the first 100 h, with a more pronounced loss observed for PE-50PT and PE-50RT samples, followed by a progressive reduction in the leakage rate until a threshold is reached after around 500 h, evidencing trends similar to those reported by Valentini *et al.*[56]. PE-50SP is the sample suffering from the lowest PCM loss (-0.6 wt.%), probably due to the highest loss during the production process, with a quite low residual effective SP content of 24.6 wt.%. The second sample in terms of resistance to PCM loss is PE-70SP/EG14 (-1.2 wt.%), with a residual effective PCM content of 56.1 wt.%, confirming that the combination of HDPE and EG for the shape stabilization of SP is very efficient, while also achieving the highest PCM content. The leakage of PE-50PT and PE-50RT is more abundant, with losses of 3.9 and 2.5 wt.%, respectively, resulting in residual effective PT and RT contents of 35 and 42 wt.% respectively. In all cases, the values are much lower than in other studies that have used HDPE to stabilize non-microencapsulated PCMs[49,54,57-59]. Thus, HDPE presents very good properties as a matrix to stabilize the considered PCMs, with the majority of PCM loss occurring during melt compounding and hot compression molding. An explanation could be the formation of polymeric layers of HDPE into the structure behaving as a barrier for the PCM penetration; hence, the PCM remains entrapped in the structure after the loss of the peripheral PCM dispersed in the specimens. Despite the 89% efficiency evaluated by DSC for PE-50RT, which can be considered quite lower than, for example, those close to 100% for only EG impregnation[23], the total leakage in the 40 days in the presence of HDPE as supporting material is very well contained. The

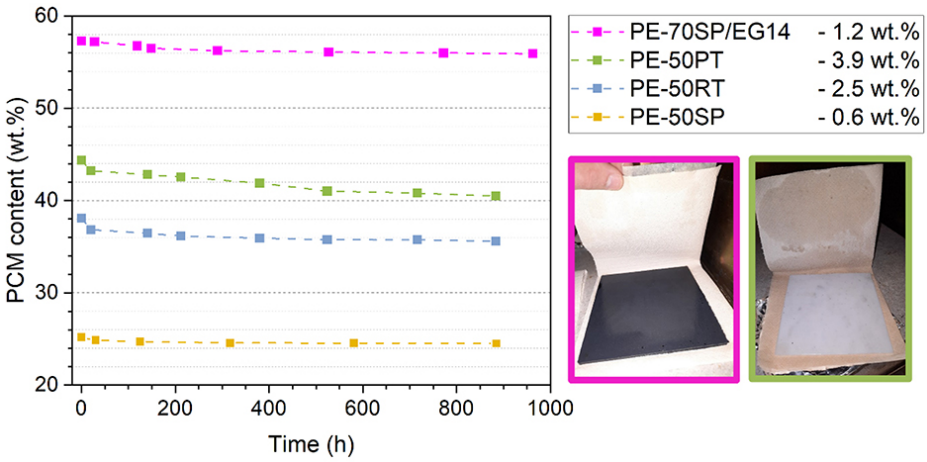

Figure 7. Leakage results at 60 °C of HDPE composites with different PCM contents.

Figure 8. PE enveloped panels having dimensions 120 × 120 × 3 mm^3 (top) and 200 × 200 × 3 mm^3 (bottom).

EG-stabilized samples[23] showed continuous PCM loss (8 to 14 wt.% in total); thus, the high impregnation efficiency was contrasted by the abundant leakage in service above melting.

By encapsulating with the PE-envelope film, leakage can be totally avoided; this solution was adopted for thermal management applications to prevent material leakage into the environment[23] and can also be used without any supporting matrix[60,61]. Moreover, with this approach, PCM-based systems are suitable for adhesively attaching to surfaces, thus avoiding the loss of adhesion that a leaked PCM layer can cause onto the surface of the plate. Examples of macro-encapsulated panels with the thermo-welded PE envelope are shown in Figure 8.

Scanning electron microscopy

Fracture surfaces of HDPE composites are investigated to gain an overview of the phase distribution. Scanning electron microscopy (SEM) micrographs at low magnifications are shown in Figure 9. From the low magnification microstructures, a homogeneous distribution of the HDPE matrix and very small PCM flakes can be observed, demonstrating the suitability of the parameters used in melt compounding to disperse the phases in the nominal composition at 50 wt.% of single PCM. The fracture surfaces show a decrease of RT, PT and SP particles in HDPE, with their effective percentages being 44%, 38% and 25%, respectively, as determined by DSC. In contrast, for PE-70SP/EG14 samples, the graphite lamellae containing entrapped SP are clearly distinguishable[27], and some heterogeneity in the phase distribution can

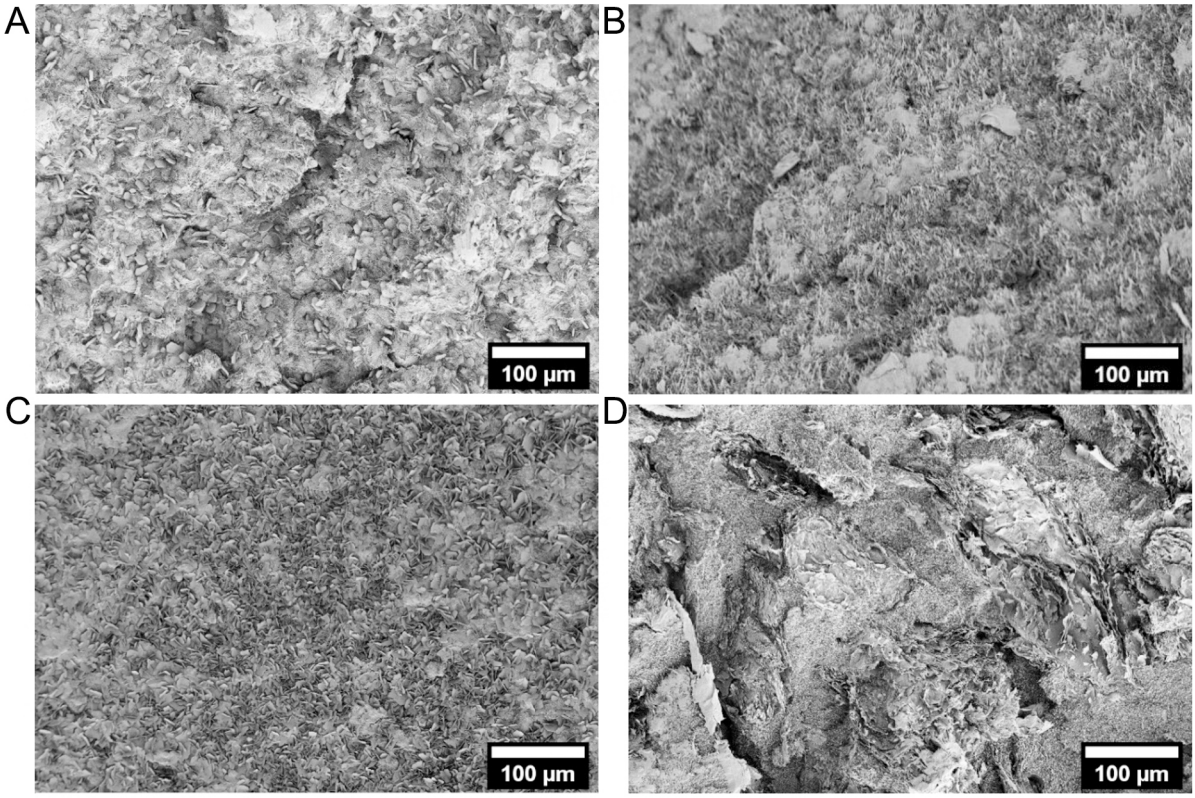

Figure 9. Overview of SEM micrographs of HDPE composites. (A) PE-50RT; (B) PE-50PT; (C) PE-50SP; (D) PE-70SP/EG14.

be observed, with even some cavities between different EG and HDPE domains, showing internal separation lines of a few hundred microns.

Higher magnification SEM micrographs, shown in Figure 10, allow for better recognition of morphologic features. The PCMs appear as micro-flakes of varying dimensions dispersed in a continuous phase of the HDPE matrix, whose filamentous fracture is evident in all compositions. Figure 10A shows RT micrometric particles with an equivalent diameter mainly between 4 and 10 microns, and a thickness in the range of 1-2 microns; some smaller particles, about 1-2 microns, could also be recognized in the HDPE domain. These different particle sizes can be related to the various melting DSC peaks. A similar aspect is also observed for PT with different groups of PCM particles dispersed in the HDPE matrix [Figure 10B]. Particles of about 1-2 microns are evident in the larger fracture domains with an almost planar morphology, whereas wider PT particles of about 3-5 microns, partially squeezed out, are visible between the elongated HDPE fibrils evidencing a ductile fracture[62].

From Figure 10C, the distinctive planar SP particles can be noticed[63], with an average width in the range of 10-25 microns and very thin lamellae, less than 0.5 microns, confirming the correct selection of the fatty acid mixture to be intercalated among the graphitic lamellae. PE-70SP/EG14 [Figure 10D] presents a more complex morphology due to the coexistence of at least three phases of three components (HDPE, PCM and EG). The nominal content of HDPE is only 30 wt.%, but the filament morphology of HDPE remains visible in the fracture zone. Moreover, the higher porosity introduced by the EG and the typical lamellar structure of EG can be observed[21,27,55].

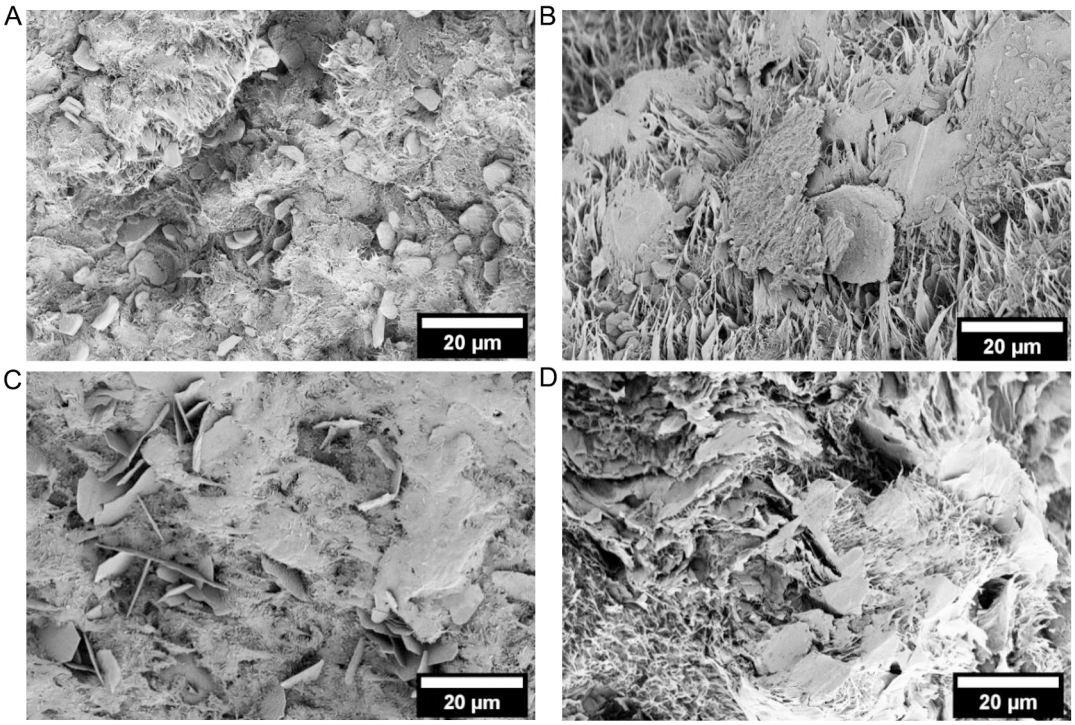

Figure 10. High magnification SEM micrographs of HDPE composites. (A) PE-50RT; (B) PE-50PT; (C) PE-50SP; (D) PE-70SP/EG14.

The various morphologies observed in SEM microscopy confirm the presence of different PCM structures, as previously discussed in DSC analysis (melting and crystallization peaks of PCM phases or domains), evidencing some porosity for PE-70SP/EG14.

Density measurements

Density analysis makes it possible to compare different morphologies and to highlight possible defects, and is reflected on the thermal conductivity both directly [see Equation (4)] and indirectly (dependence of diffusivity on void fraction). Table 6 reports the apparent densities, measured using a helium pycnometer, of neat PCMs, HDPE, EG and composite samples, along with the theoretical density values (considering the evaluated densities of the single phases and the effective contents from DSC) and the porosity evaluated with Equation (3).

The two aliphatic fatty acids SP and RT possessed a similar density of about 0.985 g/cm^3, slightly higher than that of HDPE, while the value for PT is lower than 0.9 g/cm^3. Datasheets report PCM densities in the liquid state, whose values (in the order of 0.8 g/cm^3) are coherently lower than those evaluated in the solid state due to the large volumetric expansion after melting, a characteristic typical of PCMs[1]. The density measurements of HDPE are only 0.2% lower than those provided by the producers, and this slight difference could be attributed to residual voids and/or to a lower crystallinity content of the processed polymer. EG density, measured by pressing it into pellet form, is 0.3% higher than the theoretical value of 2.26 g/cm^3 present in literature[64]. PE-50SP and PE-50PT samples present very low void fractions, while PE-50PT has a density higher than the theoretical one with a corresponding negative void fraction which has no physical sense; this can be explained by the probable presence of voids in the neat PT granules tested in the pycnometer due also to the lower measured density than the other two PCMs and the similar values of the HDPE-stabilized samples. On the other hand, a considerable void fraction (13.4%) is confirmed in PE-70SP/EG14, in agreement with the SEM observations.

Table 6. Densities and void fractions of neat raw materials and samples

Sample	ρ_{exp} (g/cm^3)	ρ_{th} (g/cm^3)	θ_v (vol.%)
RT	0.9882 ± 0.0004	-	-
PT	0.8943 ± 0.0002	-	-
SP	0.9846 ± 0.0009	-	-
HDPE	0.9529 ± 0.0006	0.955	0.2
EG	2.2670 ± 0.0070	2.26	*
PE-50RT	0.9675 ± 0.0002	0.969	0.1
PE-50PT	0.9511 ± 0.0002	0.931	**
PE-50SP	0.9594 ± 0.0003	0.961	0.2
PE-70SP/EG14	0.9954 ± 0.0004	1.149	13.4

*EG has an open structure; hence, the void fraction cannot be calculated from pycnometer measurements; **not measurable.

Specific heat capacity and thermal conductivity

In order to evaluate the best thermal performance in heat transmission, the specific heat capacity determined through DSC, bulk density and thermal diffusivity and conductivity values at 30 °C are listed in Table 7.

All the c_p values range from 1.7-2.1 J/(g·K), with the highest values observed for the PCMs and the lowest for HDPE, agreeing with datasheets and literature[65]. In the case of the PCM-HDPE blends, the c_p values are slightly lower compared to the neat PCMs, while the presence of graphite reduces the value of the PE-70SP/EG14 sample. Thermal diffusivities, presented in Table 7 and used for the thermal conductivity evaluation, exhibit the same trend as described for thermal conductivity below.

The thermal conductivity of the PCMs is in the order of 0.2 W/(m·K) at 30 °C as expected[9], while the measured thermal conductivity of HDPE is 0.5 W/(m·K), consistent with the value reported by Yang *et al.*[66]. The PCM-HDPE compounds exhibit around double thermal conductivity of the neat PCMs. To be noted, the presence of EG as a conductive filler leads to an increase of the thermal conductivity of PE-70SP/EG14 with a measured LFA value up to 1.65 ± 0.12 W/m·K, confirming that this addition is beneficial to boost the heat transfer, fundamental requirement for the PCMs usage. The corresponding enhancement relative to neat SP is about nine times greater when comparing LFA and hot disk values, respectively. This result shows a much higher improvement than those reported in most works where thermal conductivity of PCM and HDPE composites is enhanced using similar content of EG[49,54,57,59] or other conductive fillers[20,50,58,67], and is comparable only when higher EG weight fractions are used[14,66].

Limited differences between the values found using hot disk and LFA techniques can be observed. This is quite common when thermal conductivity tests are performed, as noticed and extensively treated by Weingrill *et al.*[68]; these discrepancies are not so marked and acceptable in the present study.

Measurements of the thermal conductivity above the PCM melting temperature will be possible with specific equipment due to the leakage problems of the materials, and could be the subject of future research.

Finally, the role of the PE film covering the final plates can be considered negligible due to the very low thickness (90 μm)[23] and the thermal conductivity comparable with those of the composites due to the same material of the sample matrix.

Table 7. Specific heat capacity (c_{p30}) bulk density (ρ), thermal diffusivity (α) and thermal conductivity (λ) at 30 °C measured with laser flash analysis (LFA) and hot disk (HD) according to Equation (4)

Sample	c_{p30} (J/g·K)	ρ (g/cm^3)	α_{LFA}(mm^2/s)	α_{HD}(mm^2/s)	λ_{LFA} (W/m·K)	λ_{HD} (W/m·K)
RT	1.96 ± 0.06	0.87 ± 0.03	0.122 ± 0.008	0.120 ± 0.012	0.21 ± 0.02	0.21 ± 0.01
PT	1.83 ± 0.11	0.89 ± 0.02	0.149 ± 0.001	0.166 ± 0.001	0.24 ± 0.03	0.27 ± 0.01
SP	2.10 ± 0.09	0.93 ± 0.02	0.092 ± 0.007	0.098 ± 0.001	0.18 ± 0.02	0.18 ± 0.01
PE-50RT	1.97 ± 0.04	0.96 ± 0.02	0.211 ± 0.001	0.194 ± 0.001	0.40 ± 0.02	0.37 ± 0.02
PE-50PT	1.91 ± 0.03	0.91 ± 0.01	0.227 ± 0.003	0.242 ± 0.001	0.39 ± 0.01	0.42 ± 0.02
PE-50SP	2.05 ± 0.02	0.99 ± 0.01	0.191 ± 0.005	0.141 ± 0.002	0.39 ± 0.02	0.26 ± 0.03
PE-70SP/EG14	1.71 ± 0.02	1.06 ± 0.02	0.910 ± 0.060	0.917 ± 0.007	1.65 ± 0.12	1.52 ± 0.03
HDPE	1.69 ± 0.05	0.98 ± 0.01	0.335 ± 0.011	0.294 ± 0.003	0.51 ± 0.02	0.49 ± 0.01

Compression test

The thermo-mechanical behavior of the samples was investigated through compression tests conducted at 30 and 80 °C, temperatures around 25 °C below and above the PCM melting points. The stress-strain curves of a representative specimen for each sample are reported in Figure 11, while the main results of the compressive tests are summarized in Tables 8 and 9.

Comparing Figure 11A and B, the decrease in the mechanical properties of all the samples above the PCM melting temperature is evident, showing large deformations and about half of the maximum stress due to the presence of fluid domains. The only exception is neat HDPE, for which the deterioration of the properties is much less pronounced due to the absence of molten phases. At 80 °C, a plateau can be noticed for PE-70SP/EG14 sample, from 10% to 30% strain at about 1.2 MPa.

From Table 8, the compressive elastic modulus at 30 °C of neat HDPE is the highest (72 ± 5 MPa), similar to that of PE-50PT (73 ± 0.1 MPa), and much higher than PE-50RT (49 ± 3 MPa). This demonstrates a better interaction of PT with HDPE in comparison with RT, even if more PT was lost during sample production than RT. Despite the low SP content of the PE-50SP sample, its modulus is quite lower than HDPE (62 ± 13 MPa), even if it is improved by the presence of EG (68 ± 18 MPa), also considering the highest PCM content of the PE-70SP/EG14 sample. For both SP-based samples, the values are scattered with a high standard deviation; thus, the fatty acid introduces uncertainty in the response of material, aggravated by the addition of EG. Besides the limited compressive test references available in the literature, the produced materials can be considered stiffer and more resistant than PCM/HDPE composites present in literature, such as those characterized by Nemati *et al.*[69]. A comparison with the study of Cheng *et al.* is not possible due to the absence of elastic modulus determination and the reported deformation stresses at much higher strains[67].

Neat HDPE does not reach 10% strain before the end of the test, while all other samples reach it under stress of 4 to 6 MPa; similar behavior among the specimens can be noticed by examining the stress-strain curve trends [Figure 11A]. The strain at 5 MPa of applied stress is similar for all samples, with values ranging from 8% to 9% for neat HDPE and PE-50PT, and 10% to 11.5% for the other samples.

As anticipated, at 80 °C, all compressive properties are drastically reduced, with a more pronounced effect in the presence of PCM. In fact, the mean compressive elastic modulus at 80 °C is reduced to 62.5% of its value at 30 °C for HDPE, compared to 26.5% for PE-50RT, 13.7% for PE-50PT, 25.8% for PE-50SP, and 23.5% for PE-70SP/EG14. Regarding the stresses required to achieve 10% strain, HDPE reaches it with an

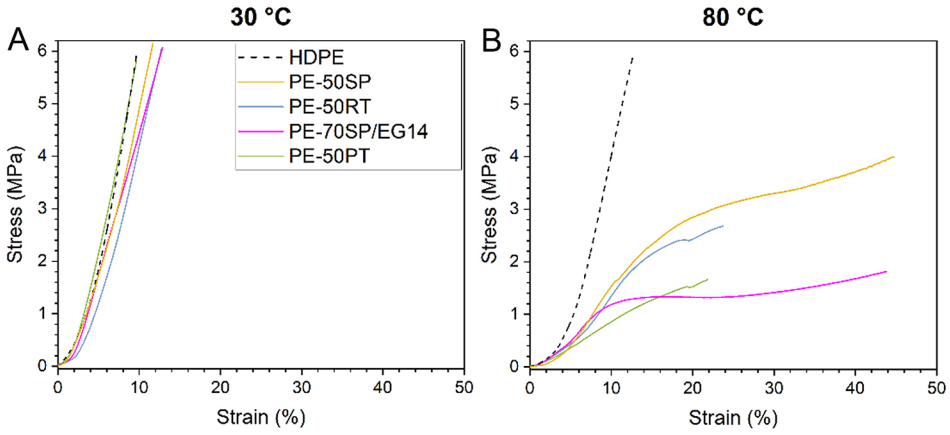

Figure 11. Stress-strain curve compression test. (A) 30 °C; (B) 80 °C.

Figure 12. Compression tested samples at 30 °C (above) and 80 °C (below). From left to right: neat HDPE, PE-50SP, PE-50RT, PE-50PT and PE-70SA/EG14.

Table 8. Results of compression tests at 30 °C

Sample	E_c (MPa)	σ_{10} (MPa)	ε_5 (%)
HDPE	72 ± 5	-	8.9 ± 0.3
PE-50RT	49 ± 3	3.7 ± 0.8	11.5 ± 0.8
PE-50PT	73 ± 1	6.0 ± 0.2	8.6 ± 0.4
PE-50SP	62 ± 13	5.1 ± 1.2	10.1 ± 1.4
PE-70SP/EG14	68 ± 18	3.9 ± 0.7	11.0 ± 2.0

E_c: Elastic compressive modulus; σ_{10}: stress at 10% of strain; ε_5: strain at 5 MPa of applied stress.

Table 9. Results of compression tests at 80 °C

Sample	E_c (MPa)	σ_{10} (MPa)	σ_{20} (MPa)	$\varepsilon_{0.5}$ (%)
HDPE	45 ± 1	3.9 ± 0.1	-	3.8 ± 0.2
PE-50RT	13 ± 4	1.3 ± 0.5	2.5 ± 0.4	5.4 ± 1.8
PE-50PT	10 ± 1	0.9 ± 0.1	1.6 ± 0.1	6.6 ± 0.2
PE-50SP	16 ± 4	1.3 ± 0.3	2.3 ± 0.5	5.9 ± 0.7
PE-70SP/EG14	16 ± 1	1.2 ± 0.1	1.5 ± 0.3	5.1 ± 0.1

E_c: Elastic compressive modulus; σ_{10}: stress at 10% of strain; σ_{20}: stress at 20% of strain; $\varepsilon_{0.5}$: strain at 0.5 MPa of applied stress.

applied stress of 3.9 ± 0.1 MPa, while the mean stresses at 80 °C are 35.2%, 15.0%, 25.5% and 30.8% of the values measured at 30 °C. Once again, the beneficial effect of EG can be noticed, considering also that PE-

70SP/EG14 presents the highest melting enthalpy [Table 5]. For the PCM/HDPE blends, the stresses double when the strain value doubles, while for PE-70SP/EG14, the stress increase is only 25%; however, HDPE never reached 20% strain. The strains at 80 °C evaluated at 0.5 MPa (one order of magnitude below the tests at 30 °C) range from 5.1% to 6.6%, except for neat HDPE (3.8% ± 0.2%).

In Figure 12, a specimen for each sample after the test is shown, underlying the spreading of the material tested at 80 °C, along with the evident permanent deformation of the specimens. None of the envelopes present any damage after the tests, confirming that the PE macro-encapsulation is a suitable technique for containing the PCM, also under unexpectedly high loads.

Three-point bending test

The flexural behavior of the materials is investigated as auxiliary information of mechanical properties for thin geometries applications. In Figure 13, a flexural stress-strain curve of one representative specimen for each sample is shown, and in Table 10 the main flexural properties are listed. HDPE remains unbroken throughout the test as shown in Figure 13, evidencing a very ductile behavior; the stress decrease after the maximum point is due to the slippage of the specimen from the supports. On the other hand the addition of PCM resulted in a lower maximum stress and embrittlement. A quite ductile behavior is also observed in PE-50SP, probably due to the low PCM fraction.

The flexural elastic modulus increases for PE-50RT (1.07 ± 0.05 GPa) and PE-50PT (1.21 ± 0.09 GPa) compared with neat HDPE (0.93 ± 0.06 GPa), while the addition of SP reduces it (0.57 ± 0.08 GPa), unless combined with EG (1.64 ± 0.04 GPa), which results in the highest reached value, again demonstrating the beneficial effect of EG in enhancing stiffness. The flexural strength is negatively affected by the addition of PCM, decreasing from 22.9 ± 0.3 MPa to values ranging between 12 and 18 MPa. EG improves this, increasing it from 12.0 ± 0.2 MPa in the PE-50SP sample to 15.1 ± 1.4 MPa in the PE-70SP/EG14 sample. The flexural strain at break follows an inverse trend relative to the PCM content in the sample: it decreases from 7.0% for neat HDPE to 1.5% for the PE-70SP/EG14 sample. Sun *et al.* obtained comparable properties for neat HDPE; however, the flexural strength and elastic modulus of the PCM composites are lower than those obtained in this study, despite their materials having a lower PCM content[33]. In the open literature, to achieve comparable flexural properties, other phases are incorporated as supporting matrices in addition to HDPE, drastically reducing the PCM content[35,37].

Vicat test

In order to evaluate the maximum using temperature, the resistance of the materials to external penetration in temperature is quantified by the Vicat Softening Temperature (*VST)* values reported in Table 11.

The penetration of 1 mm for HDPE occurs at a temperature a few degrees lower than its melting point, while in the presence of PCM it decreases by about 40-50 °C, with the exception of PE-50SP, whose *VST* of 90 ± 5 °C could be attributed to a lower amount of PCM. The lower the HDPE content, the lower the *VST*. One of the main advantages of using HDPE is the possibility to subject the composite material to temperatures higher than 95-97 °C.

Shore A hardness

The hardness of HDPE and composites was evaluated below and above the melting temperature of PCM, in order to obtain further data on the panel performance. In Table 12 the results of shore A hardness measured at 30 and 80 °C are reported.

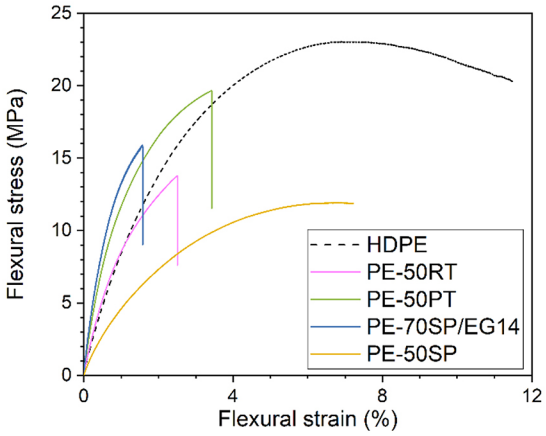

Figure 13. Flexural stress-strain curve at room temperature.

Table 10. Results of flexural tests at 23 °C

Sample	E_f (GPa)	S_f (MPa)	ε_{fb} (%)
HDPE	0.93 ± 0.06	22.9 ± 0.3	7.0 ± 0.1
PE-50RT	1.07 ± 0.05	14.3 ± 0.8	2.4 ± 0.2
PE-50PT	1.21 ± 0.09	17.8 ± 0.8	3.6 ± 0.3
PE-50SP	0.57 ± 0.08	12.0 ± 0.2	6.5 ± 0.5
PE-70SP/EG14	1.64 ± 0.04	15.1 ± 1.4	1.5 ± 0.3

E_f: Flexural elastic modulus; S_f: flexural strength; ε_{fb}:flexural strain at break.

Table 11. Vicat softening temperature (*VST*) results

Sample	*VST* (°C)
HDPE	128 ± 5
PE-50RT	81 ± 4
PE-50PT	73 ± 1
PE-50SP	90 ± 5
PE-70SP/EG14	73 ± 1

Table 12. Results of shore A Hardness tests at 30 and 80 °C

Sample	*Shore* A_{30} (-)	*Shore* A_{80} (-)
HDPE	96.2 ± 1.1	95.2 ± 2.4
PE-50RT	94.9 ± 1.3	89.0 ± 6.0
PE-50PT	96.0 ± 1.8	93.9 ± 1.8
PE-50SP	96.6 ± 1.6	87.0 ± 5.0
PE-70SP/EG14	95.1 ± 1.9	92.0 ± 4.0

The shore A hardness (ShA) at 30 °C is similar for all the samples, in the range 95-97, and at 80 °C shows a ShA decrease between 87 and 94 ShA in the presence of PCM. It is worth noting that these experimental results of Shore A at 80 °C above the melting temperature of PCM are much higher than those obtained by Ehid *et al.* (Shore A of 48 at 50 °C for blends of HDPE and 50 wt.% of paraffin), while the hardness values at ambient temperature are consistent[70].

Infrared (IR) thermography

A verification of the heat absorbance at constant temperature of the PCM-based composite materials, which is fundamental for the thermal management mechanism, is shown in Figure 14. The thermography of the sheets depicted in Figure 2 is presented during heating from 23 to 84 °C (left) and cooling with the inverse ramp (right) after 2 (A and B), 15 (C and D) and 45 (E and F) minutes.

The maintenance of the constant temperature for all the samples can be clearly observed once the PCM has molten. During cooling, a slower decrease in temperature compared to the paperboard is noticed until the recrystallization temperature of PCM is reached; at this point, the temperature remains constant until the PCM recrystallization is completed. Figure 14D shows the highest enthalpic content of PE-70SP/EG14 (right-lower corner), as indicated by the fact that, unlike the other samples, all areas of this sample remain around 50 °C, suggesting that a fraction of PCM has not yet solidified. In addition, the temperature is well-homogeneous, confirming the effectiveness of EG in improving the thermal response. After 45 min of cooling, the system reaches equilibrium at room temperature. Inhomogeneities can be observed in the materials without EG, with temperature variations across different spots in the sheets; however, the phase distribution is much more uniform compared with other PCM distributions[71]. The paperboard temperature serves as a reference, assuming the panels were composed of only HDPE.

In Figure 15, the recorded temperatures at the center of the sheet surface and on a paperboard spot during cooling are reported. The delay in reaching a certain temperature due to the presence of the PCM is evident, in the order of 30 min considering either 30 or 35 °C. The starting temperature of the supporting paperboard starts its sudden temperature decrease immediately after the remotion from the oven, while the PCM-based sheets present a much less pronounced cooling rate. At the beginning of cooling, PE-70SP/EG14 is at SP melting temperature; hence, a PCM fraction is still solid; the other samples instead are heated above 60 °C after the complete melting of the PCM, confirming the lower enthalpic content. Similarly, the lower slope of PE-70SP/EG14 temperature profile confirms a higher stored heat providing 10 min of additional delay to reach 45 °C with respect to the other samples. These delays will increase with the mass (total enthalpy)[23], in either heating (thermal management) or cooling; unfortunately, during heating, a continuous representation of the temperature with time is not possible because the IR thermo-camera must be kept outside the oven.

Comparative properties of HDPE-based panels

In view of a potential final application and considering panels 2 cm thick, the main thermo-mechanical properties of the systems are compared in Table 13 to allow a qualitative and quantitative evaluation of the performances in the material selection. The thermal management ability (*TMA*) for a panel of thickness 2 cm is expressed as an energy normalized for surface unit, as given in

$$TMA = \frac{Energy}{m^2(2\ cm)} = \Delta H_{m2} \cdot \rho \cdot V \tag{5}$$

where *Energy* is related to a panel of volume (V) 100 × 100 × 2 cm^3.

Starting with a general comparison of the thermal management plates, considering the similar densities and elastic flexural moduli, as well as maximum melting enthalpy observed in the presence of EG, the applicable temperature is higher for the composites containing larger fractions of HDPE. Furthermore, PE-70SP/EG14 exhibits the highest flexural modulus (1.6 GPa) and the best properties in terms of thermal conductivity (1.65 W/m·K) and volumetric enthalpy (112.1 J/cm^3). Additionally, it shows a narrower crystallization

Table 13. Summary of HDPE-based panels properties

Sample	ρ (g/cm^3)	E_f (GPa)	ΔH_m (J/g)	*VST* (°C)	λ_{LFA} (W/m·K)	ΔH_m^* (J/cm^3)	ΔT^+ (°C)	ΔT^- (°C)	*SD* (kg/m^2)	*TMA* (MJ/m^2)
PE-50RT	0.97	1.07	91.6	81	0.40	88.9	45-54	50-33	19.4	1.8
PE-50PT	0.95	1.21	95.1	73	0.39	90.3	46-56	54-30	19.0	1.9
PE-50SP	0.96	0.57	49.3	90	0.39	47.3	46-55	52-35	19.2	0.9
PE-70SP/EG14	1.00	1.64	112.1	73	1.65	112.1	46-57	52-40	20.0	2.2

ρ: Bulk density at 23°C; E_f: flexural elastic modulus at 23 °C; *VST*: vicat softening temperature; ΔH_m: specific melting enthalpy (2nd heating scan); λ_{LFA}: thermal conductivity determined through LFA technique at 30 °C; ΔH_m^*: melting enthalpy normalized by volume; ΔT^+: melting temperature range (heating); ΔT^-: crystallization temperature range (cooling); *SD*: surface density of a panel having thickness 20 mm; *TMA*: thermal management ability of a panel having thickness 20 mm (Equation 5).

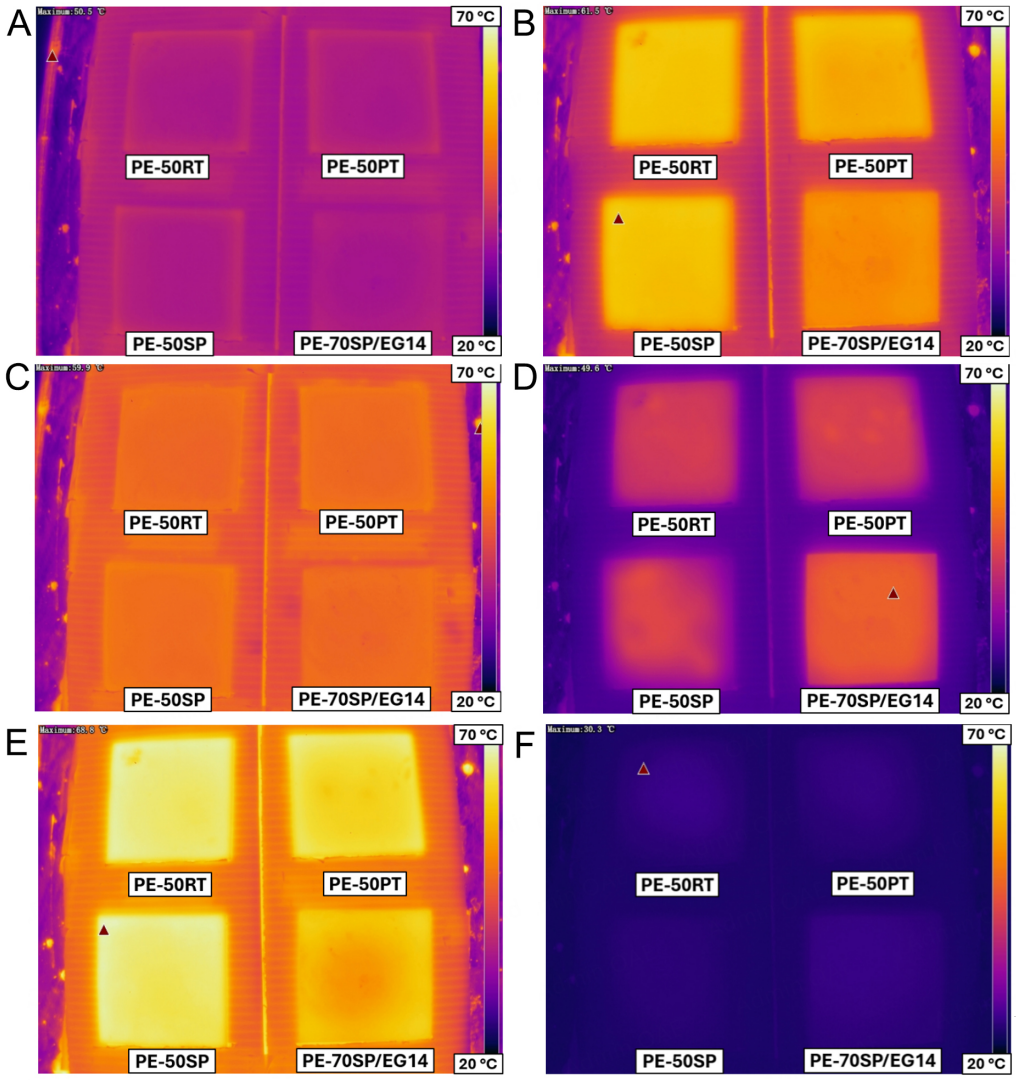

Figure 14. IR thermography images during heating (left) and cooling (right) of the sheets 120 × 120 × 3 mm^3 shown in Figure 2 after: 2 min (A and B), 15 min (C and D) and 45 min (E and F).

temperature range and the highest surface density, which contributes to the highest *TMA* value of 2.2 MJ/m^2. This value can be considered a direct indicator of the thermal performance of the panels.

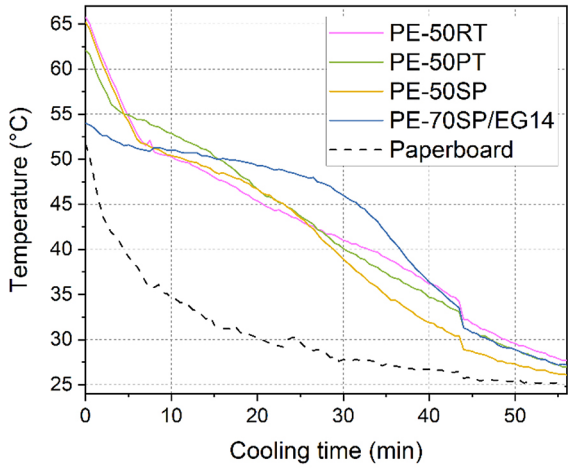

Figure 15. IR thermography temperatures in cooling.

CONCLUSIONS

HDPE has been demonstrated to be suitable for the shape stabilization of three organic PCMs with solid-liquid phase transitions close to 55 °C, which exhibit reciprocal chemical affinity and miscibility. These include organic fatty acid compound (RT), aliphatic alcohol composition (PT) or stearic-palmitic acids mixture (SP). The role of HDPE is fundamental for PCM stabilization and containing leakage. Moreover, high latent heat materials having a homogeneous phase distribution are obtained, with melting enthalpies ranging from 50 to 112 J/g. The onset and end temperatures of the melting transitions are 46 and 54-57 °C, respectively, while in cooling, the range is broader (54-30 °C), narrowing to 52-40 °C in the presence of EG. These materials can be processed as thermoplastics to form geometries suited to specific applications, e.g., sheets for electronic devices.

The fatty acid mixture (SP), which presents the lower interaction with HDPE, performs particularly well when double-stabilized with EG through vacuum impregnation, achieving an outstanding thermal conductivity nine times higher than that of the neat PCM. This innovative impregnation process enables a 3D orientation of graphite lamellae, within which the SP phase change material is intercalated, guaranteeing a continuous conductive network. This results in higher thermal conductivity than other works detailing the addition of carbonaceous fillers to PCM/HDPE composites.

RT (fatty acid) and PT (fatty alcohol) phase change materials present similar potential for shaping and stabilizing in 50 wt.% HDPE. However, the aliphatic alcohol composition (PT) shows more promising behavior due to its higher enthalpy and bio-derived nature.

An extensive and detailed mechanical characterization was performed to address the gap in the literature regarding HDPE-PCM systems for TES applications. In particular, flexural tests, Vicat, and compression and shore A hardness tests at 30 and 80 °C were conducted and compared for various materials. The heat storage mechanism was investigated through IR thermography, confirming delays proportional to the enthalpic content of the composites. In thermal management applications, the material quantity will be designed based on DSC enthalpies, ensuring sufficient heat absorption to dampen temperature peaks and/or delay the temperature rise/decrease. Comparative properties of 2 cm thick panels revealed the best properties for SP/EG in 30 wt.% of HDPE with a thermal conductivity of 1.65 W/m K, TMA of 2.2 MJ/m^2, a flexural modulus of 1.6 GPa and a thermal range 46-57 °C in heating and 52-40 °C in cooling. A larger

thermal interval in cooling (54-30 °C) was found for the PE-50PT with a flexural modulus of 1.2 GPa and TMA of 1.9 MJ/m^2. Similar properties were observed for PE-50RT with a higher VST (81 *vs.* 73 °C).

The produced 2 cm thick panels, with a surface density of about 19 kg/m^2, are good candidates in TES applications due to their excellent thermal properties, shape stability, and mechanical strength.

DECLARATIONS

Acknowledgments

The authors acknowledge Marco Guidolin and Alice Benin (Marghera, Eni S.p.A.) for the technical assistance in the preparation of PCM-EG systems. Maurizio Grigiante and Alessandro Prada (University of Trento) are kindly acknowledged for assistance in Hot Disk analysis.

Authors' contributions

Main contributions to conception and experimental design, data analysis and interpretation: Sacchet, S.; Valentini, F.; Po, R.; Fambri, L.
Data acquisition, and writing and editing: Sacchet, S.; Valentini, F.; Fambri, L.
Administrative, technical, and material support: Rizzo, C.; Po, R.; Fambri, L.

Availability of data and materials

The raw data supporting the conclusions of this article will be made available upon request from the authors.

Financial support and sponsorship

None.

Conflicts of interest

All authors declared that there are no conflicts of interest.

Ethical approval and consent to participate

Not applicable.

Consent for publication

Not applicable.

REFERENCES

1. Lawag, R. A.; Ali, H. M. Phase change materials for thermal management and energy storage: a review. *J. Energy Storage* **2022**, *55*, 105602. DOI
2. Yu, Z.; Zhang, J.; Pan, W. A review of battery thermal management systems about heat pipe and phase change materials. *J. Energy Storage* **2023**, *62*, 106827. DOI
3. Luo, J.; Zou, D.; Wang, Y.; Wang, S.; Huang, L. Battery thermal management systems (BTMs) based on phase change material (PCM): a comprehensive review. *Chem. Eng. J.* **2022**, *430*, 132741. DOI
4. Gao, Y.; Meng, X. A comprehensive review of integrating phase change materials in building bricks: Methods, performance and applications. *J. Energy Storage* **2023**, *62*, 106913. DOI
5. Sharshir, S. W.; Joseph, A.; Elsharkawy, M.; et al. Thermal energy storage using phase change materials in building applications: a review of the recent development. *Energy Build.* **2023**, *285*, 112908. DOI
6. Gao, Y.; Wu, D.; Dai, Z.; Wang, C.; Chen, B.; Zhang, X. A comprehensive review of the current status, developments, and outlooks of heat pipe photovoltaic and photovoltaic/thermal systems. *Renew. Energy* **2023**, *207*, 539-74. DOI

7. Mourad, A.; Aissa, A.; Said, Z.; Younis, O.; Iqbal, M.; Alazzam, A. Recent advances on the applications of phase change materials for solar collectors, practical limitations, and challenges: a critical review. *J. Energy Storage* **2022**, *49*, 104186. DOI
8. Shi, Y.; Zhao, Y.; Zhang, Y.; Fan, Z.; Jiang, D. Study on the reliability and stability of fatty acid-paraffin ternary phase change materials as energy-saving materials. *ChemistrySelect* **2024**, *9*, e202303114. DOI
9. Singh, P.; Sharma, R. K.; Ansu, A. K.; Goyal, R.; Sarı, A.; Tyagi, V. V. A comprehensive review on development of eutectic organic phase change materials and their composites for low and medium range thermal energy storage applications. *Solar Energy Mater. Solar Cells* **2021**, *223*, 110955. DOI
10. Wijesuriya, S.; Tabares-Velasco, P. C. Experimental apparatus and methodology to test and quantify thermal performance of micro and macro-encapsulated phase change materials in building envelope applications. *J. Energy Storage* **2020**, *32*, 101770. DOI
11. Cai, Z.; Liu, J.; Zhou, Y.; et al. Flexible phase change materials with enhanced tensile strength, thermal conductivity and photo-thermal performance. *Solar Energy Mater. Solar Cells* **2021**, *219*, 110728. DOI
12. Rollo, G.; Zullo, R.; Bonadies, I.; et al. Synergistic effect of phase change materials and reduced graphene oxide in enhancing the thermoregulating properties of polymeric composites. *J. Mater. Sci.* **2023**, *58*, 1044-58. DOI
13. Valentini, F.; Grigiante, M.; Prada, A.; Fambri, L.; Dorigato, A.; Pegoretti, A. Experimental dynamic thermal properties determination of EPDM/NBR panels with a shape stabilized phase change material based on summer daily temperatures of four cities in Italy. *Energy Build.* **2024**, *318*, 114503. DOI
14. Abdelrazeq, H.; Sobolčiak, P.; Al-Ali, A. M. M.; Ouederni, M.; Krupa, I. Recycled polyethylene/paraffin wax/expanded graphite based heat absorbers for thermal energy storage: an artificial aging study. *Molecules* **2019**, *24*, 1217. DOI PubMed PMC
15. Amin, M.; Putra, N.; Kosasih, E. A.; Prawiro, E.; Luanto, R. A.; Mahlia, T. Thermal properties of beeswax/graphene phase change material as energy storage for building applications. *Appl. Therm. Eng.* **2017**, *112*, 273-80. DOI
16. Du, B.; Wang, M.; Zhao, Q.; Hu, X.; Ding, S. Phase change materials microcapsules reinforced with graphene oxide for energy storage technology. *Energy Mater.* **2023**, *3*, 300026. DOI
17. Gao, H.; Bing, N.; Xie, H.; Yu, W. Energy harvesting and storage blocks based on 3D oriented expanded graphite and stearic acid with high thermal conductivity for solar thermal application. *Energy* **2022**, *254*, 124198. DOI
18. Singh, P.; Sharma, R. K.; Khalid, M.; Goyal, R.; Sarı, A.; Tyagi, V. V. Evaluation of carbon based-supporting materials for developing form-stable organic phase change materials for thermal energy storage: a review. *Solar Energy Mater. Solar Cells* **2022**, *246*, 111896. DOI
19. Qu, Y.; Wang, S.; Tian, Y.; Zhou, D. Comprehensive evaluation of Paraffin-HDPE shape stabilized PCM with hybrid carbon nano-additives. *Appl. Therm. Eng.* **2019**, *163*, 114404. DOI
20. Jaiswal, S. J.; Sonare, S. N.; Mahanwar, P. A. Thermal energy storage material based on high density polyethylene filled with graphene oxide modified microencapsulated eutectic mixture of fatty acid. *J. Polym. Environ.* **2024**, *32*, 150-63. DOI
21. Pea HJ, An Z, Du X, Shi T, Zhang D. Structure, characterization and thermal properties of the form-stable paraffin/high-density polyethylene/expanded graphite/epoxy resin composite PCMs for thermal energy storage. *J. Therm. Sci.* **2023**, *32*, 2104-14. DOI
22. Hong, Y. Preparation of polyethylene-paraffin compound as a form-stable solid-liquid phase change material. *Solar Energy Mater. Solar Cells* **2000**, *64*, 37-44. DOI
23. Sacchet, S.; Valentini, F.; Benin, A.; Guidolin, M.; Po, R.; Fambri, L. Expanded graphite (EG) stabilization of stearic and palmitic acid mixture for thermal management of photovoltaic cells. *C* **2024**, *10*, 46. DOI
24. Rahmalina, D.; Rahman, R. A.; Ismail Maintaining high thermal response of carbon nanotubes after melting intensification in solid-liquid heat storage system. *Carbon Trends* **2023**, *13*, 100294. DOI
25. Chai, S.; Sun, K.; Zhao, D.; Kou, Y.; Shi, Q. Form-stable erythritol/HDPE composite phase change material with flexibility, tailorability, and high transition enthalpy. *ACS Appl. Polym. Mater.* **2020**, *2*, 4464-71. DOI
26. Nawaz, K.; Freeman, T. B.; Rodriguez, R. M.; Boetcher, S. K. S. Moisture affinity of HDPE/phase-change material composites for thermal energy storage applications. *RSC Adv.* **2021**, *11*, 30569-73. DOI PubMed PMC
27. Wang, H.; Rao, Z.; Li, L.; Liao, S. A novel composite phase change material of high-density polyethylene/d-mannitol/expanded graphite for medium-temperature thermal energy storage: characterization and thermal properties. *J. Energy Storage* **2023**, *60*, 106603. DOI
28. Rahmalina, D.; Rahman, R. A.; Ismail Improving the phase transition characteristic and latent heat storage efficiency by forming polymer-based shape-stabilized PCM for active latent storage system. *Case Stud. Therm. Eng.* **2022**, *31*, 101840. DOI
29. Rahmalina, D.; Rahman, R. A.; Ismail Increasing the rating performance of paraffin up to 5000 cycles for active latent heat storage by adding high-density polyethylene to form shape-stabilized phase change material. *J. Energy Storage* **2022**, *46*, 103762. DOI
30. Suyitno, B. M.; Pane, E. A.; Rahmalina, D.; Rahman, R. A. Improving the operation and thermal response of multiphase coexistence latent storage system using stabilized organic phase change material. *Results Eng.* **2023**, *18*, 101210. DOI
31. Suyitno, B. M.; Rahmalina, D.; Ismail, I.; Rahman, R. A. Superior long-term performance of composite phase change material with high-density polyethylene under thermal aging process. *RCMA* **2023**, *33*, 145-51. DOI
32. Tarigond, H.; Reddy, R. M.; Maheswari, C. U.; Reddy, E. S. Effect of iron scrap additives in stearic acid as PCM for thermal energy storage system. *J. Therm. Anal. Calorim.* **2020**, *141*, 2497-510. DOI
33. Sun, J.; Zhao, J.; Zhang, W.; et al. Composites with a novel core-shell structural expanded perlite/polyethylene glycol composite PCM as novel green energy storage composites for building energy conservation. *Appl. Energy.* **2023**, *330*, 120363. DOI
34. Grzybek, J.; Nazari, M.; Jebrane, M.; et al. Bio-based phase change material for enhanced building energy efficiency: a study of beech

and thermally modified beech wood for wall structures. *Energy Storage* **2024**, *6*, e568. DOI

35. Guo, X.; Jiang, H.; Qiu, C.; et al. An energy storage composite using cellulose grafted polyethylene glycol as solid-solid phase change material. *Polym. Composites* **2024**, *45*, 1524-33. DOI
36. Salgado-Pizarro, R.; Ulldemolins, G.; Navarro, M. E.; et al. New shape-stabilized phase change materials obtained by single-screw extruder. *Energy Storage* **2021**, *3*, e268. DOI
37. Xu, J.; Sun, J.; Zhao, J.; et al. Eco-friendly wood plastic composites with biomass-activated carbon-based form-stable phase change material for building energy conversion. *Ind. Crop. Prod.* **2023**, *197*, 116573. DOI
38. Data and Facts. Available from: https://www.ise.fraunhofer.de/en/publications/studies/photovoltaics-report.html [Last accessed on 14 Jan 2024].
39. Nelson, A.; Mateti, S.; Chen, Y.; Sharma, N.; Han, Q.; Rahman, M. M. Creating value added nano silicon anodes from end-of-life photovoltaic modules: recovery, nano structuring, and the impact of ball milling and binder on its electrochemical performance. *Energy Mater.* **2024**, *4*, 400046. DOI
40. Sabatino M, Hendawi R, Garcia AS. Silicon solar cells: trends, manufacturing challenges, and AI perspectives. *Crystals* **2024**, *14*, 167. DOI
41. Al-Yasiri, Q.; Szabó, M. Building envelope-combined phase change material and thermal insulation for energy-effective buildings during harsh summer: simulation-based analysis. *Energy Sustain. Dev.* **2023**, *72*, 326-39. DOI
42. Singh, R. P.; Kaushik, S.; Rakshit, D. Performance evaluation of charging process in a cascade latent heat storage system (C-LHSS) based on heat flux DSC results. *Int. J. Therm. Sci.* **2020**, *151*, 106274. DOI
43. Standard test method for determining specific heat capacity by differential scanning calorimetry. Available from: https://www.astm.org/e1269-11.html [Last accessed on 14 Jan 2024].
44. ISO 22007-2:2022. Available from: https://www.iso.org/standard/81836.html [Last accessed on 14 Jan 2024].
45. ISO 844:2021. Available from: https://www.iso.org/standard/73560.html [Last accessed on 14 Jan 2024].
46. Standard test methods for flexural properties of unreinforced and reinforced plastics and electrical insulating materials. Available from: https://www.astm.org/standards/d790 [Last accessed on 14 Jan 2024].
47. Standard test method for vicat softening temperature of plastics. Available from: https://www.astm.org/d1525-17e01.html [Last accessed on 14 Jan 2024].
48. Standard test method for rubber property - durometer hardness. Available from: https://www.astm.org/d2240-15r21.html [Last accessed on 14 Jan 2024].
49. Xie, Y.; Yang, Y.; Liu, Y.; et al. Paraffin/polyethylene/graphite composite phase change materials with enhanced thermal conductivity and leakage-proof. *Adv. Compos. Hybrid. Mater.* **2021**, *4*, 543-51. DOI
50. Chen, Y.; Zhang, H.; Xu, C.; Cong, R.; Fang, G. Thermal properties of 1-hexadecanol/high density polyethylene/graphene nanoplates composites as form-stable heat storage materials. *Solar Energy Mater. Solar Cells* **2022**, *237*, 111580. DOI
51. Kolařík, J.; Fambri, L.; Šlouf, M.; Konečný, D. Heterogeneous polyamide 66/syndiotactic polystyrene blends: phase structure and thermal and mechanical properties. *J. Appl. Polym. Sci.* **2005**, *96*, 673-84. DOI
52. Michell, R. M.; Müller, A. J. Confined crystallization of polymeric materials. *Prog. Polym. Sci.* **2016**, *54-5*, 183-213. DOI
53. He, L.; Wang, M.; Zhang, X.; et al. The confinement effect on phase change materials by physicochemical structure of wood-based materials. *Ind. Crops. Prod.* **2024**, *212*, 118299. DOI
54. Zhao, J.; Li, Y.; Fang, X.; et al. High interface compatibility and phase change enthalpy of heat storage wood plastic composites as bio-based building materials for energy saving. *J. Energy Storage* **2022**, *51*, 104293. DOI
55. Zhou, R.; Ming, Z.; He, J.; Ding, Y.; Jiang, J. Effect of magnesium hydroxide and aluminum hydroxide on the thermal stability, latent heat and flammability properties of paraffin/HDPE phase change blends. *Polymers* **2020**, *12*, 180. DOI PubMed PMC
56. Valentini, F.; Fambri, L.; Dorigato, A.; Pegoretti, A. Production and characterization of TES-EPDM foams with paraffin for thermal management applications. *Front. Mater.* **2021**, *8*, 660656. DOI
57. Nishad, S.; Mohammed, H.; Sobolciak, P.; Krupa, I. Evaluation of photothermal conversion performance of shape-stabilized phase change materials using a heat flux evolution curve. *J. Mater. Res. Technol.* **2023**, *24*, 3717-30. DOI
58. Yadav, D. K.; Rathore, P. K. S.; Singh, R. K.; Gupta, A. K.; Sikarwar, B. S. Experimental study on paraffin wax and soya wax supported by high-density polyethylene and loaded with nano-additives for thermal energy storage. *Energies* **2024**, *17*, 2461. DOI
59. Qu, Y.; Wang, S.; Zhou, D.; Tian, Y. Experimental study on thermal conductivity of paraffin-based shape-stabilized phase change material with hybrid carbon nano-additives. *Renew. Energy* **2020**, *146*, 2637-45. DOI
60. Venkitaraj, K. P.; Suresh, S.; Praveen, B.; Nair, S. C. Experimental heat transfer analysis of macro packed neopentylglycol with CuO nano additives for building cooling applications. *J. Energy Storage* **2018**, *17*, 1-10. DOI
61. Zukowski, M. Experimental study of short term thermal energy storage unit based on enclosed phase change material in polyethylene film bag. *Energy Convers. Manag.* **2007**, *48*, 166-73. DOI
62. Messenger, M. A.; Troxler, C. J.; Melendez, I.; et al. Mechanical and thermal characterization of phase-change material and high-density polyethylene functional composites for thermal energy storage. *J. Solar Energy Eng.* **2023**, *145*, 061006. DOI
63. Pan, S.; Zhou, J.; Li, H.; Quan, C. Particle formation by supercritical fluid extraction and expansion process. *Sci. World J.* **2013**, *2013*, 538584. DOI PubMed PMC
64. Vohler, O.; Von Sturm, F.; Wege, E.; Frohs, W. Industrial carbon and graphite materials, Volume I: raw materials, production and applications. WILEY-VCH GmbH; 2021. Available from: https://onlinelibrary.wiley.com/doi/book/10.1002/9783527674046 [Last

accessed on 14 Jan 2024]

65. Van Krevelen, D. W.; Te Nijenhuis, K.; Wege, E.; Frohs, W. Properties of polymers (Fourth Edition). Amsterdam: Elsevier; 2009. Available from: https://www.sciencedirect.com/book/9780080548197/properties-of-polymers [Last accessed on 14 Jan 2024]
66. Yang, C.; Navarro, M. E.; Zhao, B.; et al. Thermal conductivity enhancement of recycled high density polyethylene as a storage media for latent heat thermal energy storage. *Solar Energy Mater. Solar Cells* **2016**, *152*, 103-10. DOI
67. Cheng, F.; Xu, Y.; Lv, Z.; et al. Form-stable and tough paraffin-Al_2O_3/high density polyethylene composites as environment-friendly thermal energy storage materials: preparation, characterization and analysis. *J. Therm. Anal. Calorim.* **2021**, *146*, 2089-99. DOI
68. Weingrill, H.; Hohenauer, W.; Resch-Fauster, K.; Zauner, C. Analyzing thermal conductivity of polyethylene-based compounds filled with copper. *Macro. Mater. Eng.* **2019**, *304*, 1800644. DOI
69. Nemati, S.; Pircheraghi, G. Fabrication of a form-stable phase change material with green fatty acid and recycled silica nanoparticles from spent lead-acid battery separators with enhanced thermal conductivity. *Thermochim. Acta.* **2020**, *693*, 178781. DOI
70. Ehid, R.; Fleischer, A. S. Development and characterization of paraffin-based shape stabilized energy storage materials. *Energy Convers. Manag.* **2012**, *53*, 84-91. DOI
71. Sorze, A.; Valentini, F.; Dorigato, A.; Pegoretti, A. Salt leaching as a green method for the production of polyethylene foams for thermal energy storage applications. *Polym. Eng. Sci.* **2021**. DOI